

**Superconductor to weak-insulator transitions in disordered tantalum nitride films**Nicholas P. Breznay,<sup>1,2,\*</sup> Mihir Tendulkar,<sup>1</sup> Li Zhang,<sup>1</sup> Sang-Chul Lee,<sup>3</sup> and Aharon Kapitulnik<sup>1,4</sup><sup>1</sup>*Department of Applied Physics, Stanford University, Stanford, California 94305, USA*<sup>2</sup>*Department of Physics, Harvey Mudd College, Claremont, California 91711, USA*<sup>3</sup>*Department of Materials Science and Engineering, Stanford University, Stanford, California 94305, USA*<sup>4</sup>*Department of Physics, Stanford University, Stanford, California 94305, USA*

(Received 29 May 2017; revised manuscript received 10 October 2017; published 31 October 2017)

We study the two-dimensional superconductor-insulator transition (SIT) in thin films of tantalum nitride. At zero magnetic field, films can be disorder-tuned across the SIT by adjusting thickness and film stoichiometry; insulating films exhibit classical hopping transport. Superconducting films exhibit a magnetic-field-tuned SIT, whose insulating ground state at high field appears to be a quantum-corrected metal. Scaling behavior at the field-tuned SIT shows classical percolation critical exponents  $z\nu \approx 1.3$ , with a corresponding critical field  $H_c \ll H_{c2}$ , the upper critical field. The Hall effect exhibits a crossing point near  $H_c$ , but with a nonuniversal critical value  $\rho_{xy}^c$  comparable to the normal-state Hall resistivity. We propose that high-carrier-density metals will always exhibit this pattern of behavior at the boundary between superconducting and (trivially) insulating ground states.

DOI: [10.1103/PhysRevB.96.134522](https://doi.org/10.1103/PhysRevB.96.134522)**I. INTRODUCTION**

Disordered two-dimensional (2D) electron systems such as amorphous thin films are commonly assumed to be either insulating (I) or superconducting (S) as the temperature  $T$  approaches zero. Crossing this S-I phase boundary by controlling disorder or magnetic field was predicted to realize a quantum phase transition, the superconductor-insulator transition (SIT) [1]. Early experimental and theoretical studies of the SIT addressed the nature of an amplitude or phase dominated transition (see Ref. [2] for reviews) while more recently, evidence for unconventional ground states proximal to the SIT has emerged. These include metallic phases [3–5] precluded by the scaling theory of localization [6] as well as a bosonic “Cooper-pair insulator” ground state [7–9]. Further, the nature of the transition itself shows different regimes of behavior with changes in the degree of material disorder.

The limit of strong disorder [10] reveals a direct, self-dual superconductor to bosonic-insulator transition [11,12]. When disorder is weak and the normal state shows quantum-corrected metallic behavior, the field-tuned SIT shows distinct critical behavior from the strong-disorder case [3,13] that is interrupted as  $T \rightarrow 0$  by a still unexplained and controversial metallic state. Observed in a range of amorphous [14–16] and crystalline [17,18] materials, a theoretical consensus has yet to emerge to explain this metallic behavior [19–23]. Recent experiments find zero Hall effect in this phase that is suggestive of particle-hole symmetry; along with the absence of a cyclotron resonance in finite-frequency studies, these results confirm it to be of “failed” superconducting character [24,25]. What separates the strong- and weak-disorder behavior regimes remains unclear, and may be due to the inhomogeneous and/or granular nature of the disorder, or microscopic properties of the proximal normal or superconducting states. As yet there are few examples where careful control of the materials system can be combined with studies across both the disorder- and field-tuned SIT.

The field- and disorder-driven suppression of superconductivity has been studied in 2D intermetallic films, such as NbSi, TiN, NbN, MoGe, and amorphous indium oxide (InO<sub>x</sub>) [13,26–29]. Notably, TiN shows what appears to be a direct field-tuned SIT and unexpected metallic saturation in the high-field insulating state [30], while both NbSi and NbN can be tuned via thickness or composition across the disorder-driven SIT [31,32]. While TaN has not been studied to date, Ta thin films show a metal intervening in the SIT as a function of field and disorder. Qin *et al.* [15] studied field-tuned transitions of several nm thick Ta films, observing hysteretic I-V characteristics and metallic saturation of the resistance at low temperature similar to that observed in MoGe [3] and arguing that it is not a simple heating effect [33]. In subsequent work [34], I-V characteristics were used to identify superconducting, metallic, and insulating behavior, while very recent studies have examined critical scaling in both the superconducting and metallic phases [35]. In pure Ta there is no direct SIT; a metallic phase appears to intervene at all disorder strengths accessible by tuning the film thickness. These differences between materials families raise a central issue: how the SIT evolves under alternative disorder tuning parameters.

Here we study a strongly spin-orbit coupled binary metal nitride system, amorphous tantalum nitride ( $a$ -TaN<sub>x</sub>), where the disorder can be controlled by tuning film thickness and composition. The most disordered films show hopping transport at low temperatures, with no evidence for superconductivity. Weakly superconducting films can be driven into an insulating state above an applied magnetic field  $H_c$ , and show a temperature-independent crossing point at  $H_c$  and finite-size scaling in  $\rho_{xx}$  that is the hallmark of the SIT. We also report similar crossing and weak scaling behavior in the Hall effect  $\rho_{xy}$ , previously observed only in InO<sub>x</sub> [36], with a nonuniversal value for the critical Hall resistivity  $\rho_{xy}^c$ . Along with evidence for unusual metallic behavior on the insulating side of the field-tuned SIT, similarities with other materials point towards a universal superconductor–weak-insulator transition (SWIT). Finally, as normal-state Hall effect data indicate metallic carrier concentrations for all superconducting films ( $n \sim 10^{23} \text{ cm}^{-3}$ ) comparable to MoGe, Ta, and other SWIT

\*nbreznay@hmc.edu

materials, we hypothesize that such large carrier densities preclude observation of a self-dual, bosonic SIT.

This article is organized as follows: sample growth and characterization data are presented in Sec. II, while low-temperature transport data and the disorder-tuned SIT are described in Sec. III. The behavior in the vicinity of the field-tuned SIT is described in Sec. V, with scaling analyses considered in detail in Sec. VI. Section VII describes the Hall effect in the vicinity of the field-tuned SIT, where a crossing point and faint scaling appears above the critical field  $H_c$ . Finally, Sec. VIII summarizes the disorder and field-tuned SIT phenomenology in  $a$ - $\text{TaN}_x$  and discusses their implications.

## II. FILM GROWTH AND CHARACTERIZATION

We study reactively sputtered  $a$ - $\text{TaN}_x$  films, most with thickness  $d \sim 5$ –20 nm, as described in part in previous work [37,38]. Reactive sputtering with a tantalum target in a background Ar/ $\text{N}_2$  mixture is a common technique for growth of TaN films [39–41]. In sputtered films, superconductivity with  $T_c$  between 5 and 10 K has been shown to be stable for a range of nitrogen stoichiometries [42]; thick films can show  $T_c$  values as high as 10.9 K [42–45]. Eight films (labeled N0–N7) were grown using a commercial AJA reactive magnetron sputtering tool and pure Ta target in flowing Ar- $\text{N}_2$  gas. The Ar/N ratio controls the film Ta/N stoichiometry (and related film properties, such as the room temperature value of  $\rho_{xx}$ ) [39–41]. Base pressure of the sputter deposition system was  $\approx 10^{-8}$  torr. Films were co-deposited onto several substrate materials, including intrinsic Si, Si with  $\text{SiO}_2$  and  $\text{Si}_3\text{N}_4$  buffer layers, and glass; aside from few-percent quantitative differences in film properties (such as the room temperature resistivity  $\rho_{xx}$ ) we found no sensitivity of film parameters to the choice of substrate. All substrates were Ar-ion plasma cleaned before sputtering. Pure Ta (and Ta-rich) films were also sputtered in identical conditions and show comparable behavior to previous studies [15]; results from one Ta-rich film (N3) are included below for comparison.

Several parameters can be used to tune to the disorder in  $a$ - $\text{TaN}_x$  (as reflected, for example, by  $\rho_{xx}$  at room temperature), including thickness,  $\text{N}_2$  partial pressure (and therefore stoichiometry  $x$ ), and other synthesis conditions. Here we control the effective film disorder by changing the thickness and (for the  $d \sim 5$  nm films) nitrogen stoichiometry. Table I shows the film growth and characterization parameters, including

TABLE I. Disordered  $\text{TaN}_x$  film electronic and structural properties, including the stoichiometry  $x$ , thickness  $d$ , superconducting transition temperature  $T_c$ , longitudinal sheet resistivity  $\rho_{xx}$ , low-field Hall coefficient  $R_H$ , and carrier density  $n$ .

Sample Name	SC/Ins.	$\text{TaN}_x$ stoichiometry $x$	$d$ (nm)	$T_c$ (K)	$\rho_{xx}$ (300 K) ( $\Omega/\square$ )	$R_H$ ( $\Omega/T$ )	$n$ ( $10^{22} \text{ cm}^{-3}$ )
N0	SC	$1.0 \pm 0.1$	250	6.4	10.6		
N1	SC	$1.1 \pm 0.1$	36	3.7	507	0.0022	7.9
N2	SC	$1.0 \pm 0.1$	4.0	2.8	828	0.014	11.1
N3	SC	$0.1 \pm 0.1$	4.9	0.5	526	0.029	4.4
N4	SC	$1.1 \pm 0.2$	5.9	0.7	$1.3 \times 10^3$	0.011	9.6
N5	Ins.	$1.2 \pm 0.2$	5.3		$8.0 \times 10^3$		
N6	Ins.	$1.4 \pm 0.2$	4.9		$13 \times 10^3$		
N7	Ins.	$1.6 \pm 0.2$	5.2		$1.4 \times 10^6$		

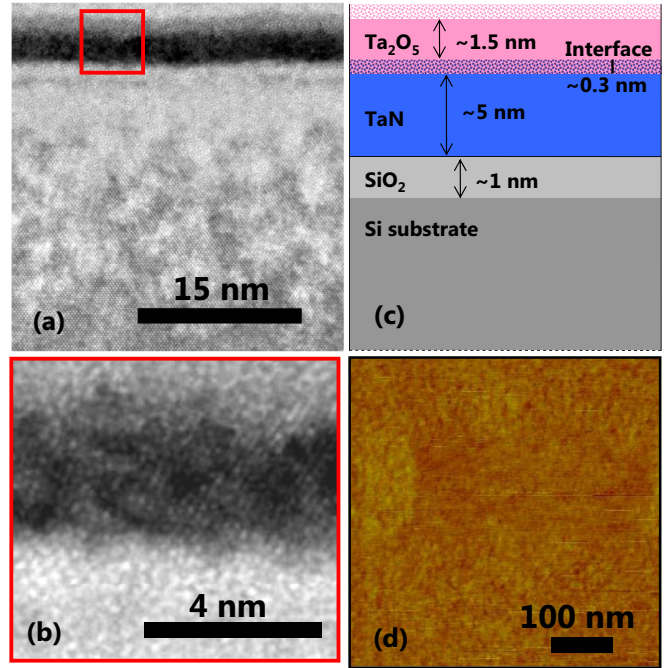


FIG. 1. (a) Cross-sectional TEM image of  $a$ - $\text{TaN}_x$  film on Si substrate, along with (b) inset showing the  $\sim 4$  nm thick amorphous film. (c) Schematic diagram of the film composition and structure based on TEM and x-ray analyses. (d) AFM image with roughness of 0.2 nm; the full range of the color scale is 2 nm.

the stoichiometry  $x$ , thickness  $d$ , and electronic properties (discussed further below).

We characterize the film thickness, morphology, chemical composition, and homogeneity with a range of techniques. TEM measurements (Fig. 1) reveal the homogeneous and disordered  $a$ - $\text{TaN}_x$  film in sample N2 on a Si substrate; this film is 4 nm thick and approximately stoichiometric. The film cross section is enlarged in Fig. 1(b); the scale bar in this panel is 4 nm. X-ray photoelectron spectroscopy (XPS) measurements confirm the film stoichiometries, with an accuracy of  $\approx 10\%$ , shown in Table I; depth profiling uncovers a  $\sim 1$  nm surface oxide layer on all films. A schematic of the film cross section including the Si substrate,  $a$ - $\text{TaN}_x$  film, along with interfacial  $\text{SiO}_2$  and  $\text{TaO}_x$  layers (with roughness  $\sim 0.5$  nm) is shown in Fig. 1(c). Scanning atomic-force microscopy measurements, shown in Fig. 1(d) for sample N2, show excellent homogeneity

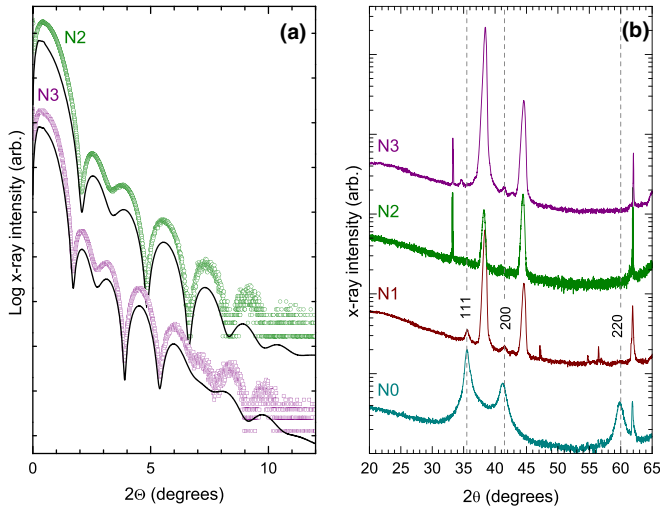


FIG. 2. (a) X-ray reflectivity scans for samples N2 and N3, along with fits (solid lines). (b) X-ray diffraction  $\theta$ - $2\theta$  scan of samples N0–N3; curves have been vertically offset for clarity. Only sample N0 shows broad (111), (200), and (220) peaks associated with fcc-TaN; peaks visible for films N1–N3 are due to the substrate or surface TaO<sub>x</sub> layer.

in the film thickness. The rms roughness is 0.1 nm ( $\approx 2\%$  of the TaN layer thickness) over a  $\sim 1 \mu\text{m}^2$  region, with no evidence for granularity or inhomogeneity on this scale. [The full range of the color scale in Fig. 1(d) is 2 nm.] Scanning electron microscope imaging also showed no sign of inhomogeneity down to the 10 nm length scale.

Figure 2(a) presents x-ray reflectivity data for two films (N2 and N3) and best-fit model curves (continuous lines). The nonlinear curve fitting analysis also yields a density  $\rho(\text{TaN}) \approx 15.9 \text{ g/cm}^{-3}$  for N2, approximately that observed in bulk samples. Film phase and composition were also analyzed using x-ray diffraction, shown in Fig. 2(b), which confirm the amorphous nature of the  $a\text{-TaN}_x$  films studied here. Broad amorphous peaks at  $36^\circ$ ,  $42^\circ$ , and  $60^\circ$  corresponding to the (111), (200), and (220) peaks of fcc  $\delta\text{-TaN}$  are visible in the curve for the thickest (250 nm) sample N0. The curve for sample N1 (36 nm) barely shows the same fcc  $\delta\text{-TaN}$  peaks, as well as peaks at  $38^\circ$  and  $44^\circ$  from orthorhombic Ta<sub>2</sub>O<sub>5</sub> (often seen for sputtered TaN<sub>x</sub> films [46]), arising from the surface tantalum oxide layer noted previously. The most thin ( $d \sim 4\text{--}5$  nm) films show additional sharp peaks from the Si substrate, but no sign of crystalline order from the  $a\text{-TaN}_x$  layer. Sample N3, with  $x \approx 0.1$ , shows behavior comparable to pure Ta films that have been studied previously.

In summary, films studied here are amorphous, continuous, and homogeneously disordered. This is reflected in the electronic properties, which show disorder-limited length scales comparable to or (as with the mean-free path  $\ell$ ) smaller than the film thickness.

### III. EXPERIMENTAL DETAILS AND SUPERCONDUCTOR-INSULATOR TRANSITION

Films were patterned into Hall-bar geometry devices (see the inset of Fig. 3) and measured using standard low-frequency

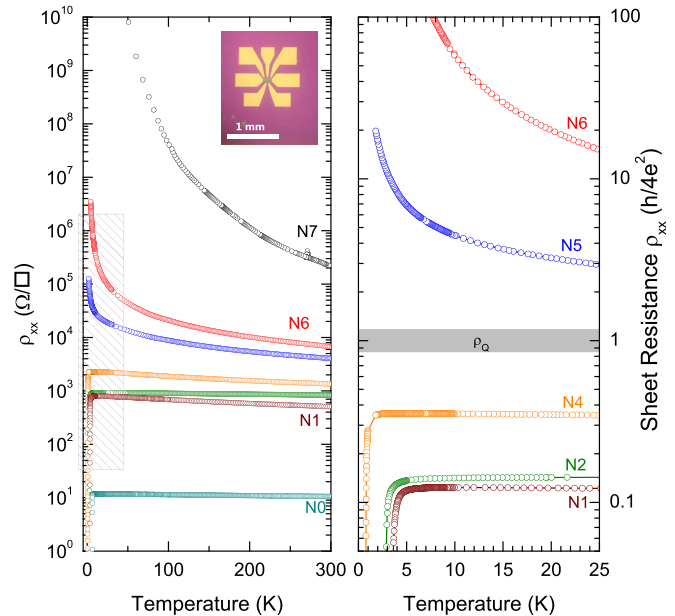


FIG. 3. Sheet resistance versus temperature for a series of disordered  $a\text{-TaN}_x$  films, along with a device schematic (inset). Disorder increases with decreasing thickness or increasing nitrogen concentration  $x$ . The hatched region at left is plotted in the panel at right, where the horizontal gray bar indicates  $\rho_Q = 6.45 \text{ k}\Omega$ .

techniques; see Ref. [37] for additional experimental details. All applied magnetic fields  $H$  were perpendicular to the film plane. Care was taken to avoid electron heating during measurements below 1 K and during magnetic field ramps; all  $\rho_{xx}$  and  $\rho_{xy}$  measurements were confirmed to be ohmic. Reported longitudinal resistivities  $\rho_{xx}$  and Hall resistivities  $\rho_{xy}$  are 2D (sheet) quantities, unless explicitly noted otherwise. Table I shows electrical transport data for the seven  $a\text{-TaN}_x$  films discussed here, four superconducting (N0, N1, N2, N4) and three insulating (N5–N7). Here  $T_c$  is determined where  $\rho_{xx}$  has fallen to 1% of the normal-state value. Also shown are the 300 K  $\rho_{xx}$ , Hall coefficient  $R_H$ , and the carrier density  $n$  estimated using a single parabolic band model appropriate for these strongly disordered films.

Hall measurements show  $\rho_{xy}$  linear in field and generally  $n$ -type carrier densities  $\sim 10^{23} \text{ cm}^{-3}$ , reported in Table I. Previous studies observed a change from  $n$  to  $p$  carrier type at  $x \sim 1.67$  [47]. Bulk film resistivities are as low as  $\rho_{xx} \sim 1 \text{ m}\Omega \text{ cm}$ , depending on the stoichiometry, again comparable to films on the boundary of the stoichiometry-tuned metal-insulator transition [47]. The mean-free paths for superconducting films are  $\ell \sim 0.1 \text{ nm}$ , with  $k_F \ell \sim 1.0\text{--}3.0$ ; here  $k_F$  is the Fermi wave vector. With the exception of the  $d \sim 250 \text{ nm}$  thick sample N0, all films can be considered 2D in the context of superconductivity ( $\xi < d$ ) and disorder-induced localization ( $L_\phi < d$ ) effects [37,38].

Figure 3 shows the resistivity for all films as a function of temperature and illustrates the distinct superconducting and insulating ground states available to these materials as the disorder is changed. Similar behavior is observed in materials where the transition is tuned by thickness (such as in Bi [48]) or otherwise controlling the disorder (e.g., TiN [5]). The

separatrix between superconducting and insulating curves is  $\rho_Q = h/4e^2$ , highlighted in the right panel of Fig. 3 that shows the low-temperature region near  $\rho_Q$ . The superconducting  $T_c$  of sputtered TaN films has been reported as high as  $\sim 11$  K for thick films [42–45]; the maximum  $T_c$  observed here is 6.9 K for the thickest (250 nm) film studied, N0.

#### IV. ZERO-FIELD GROUND STATES

Here we characterize the superconducting and insulating ground states of the  $a$ -TaN $_x$  films in the absence of an applied field, as the disorder is tuned via nitrogen stoichiometry and thickness. Beginning with the highest-disorder samples, Fig. 3 shows strong insulating behavior for samples N5–N7, with  $\rho_{xx}$  increasing exponentially with temperature. The upper panel of Fig. 4 shows  $\rho_{xx}(T)$  plotted versus  $T^{-1/2}$ , along with straight-line fits of the Efros-Shklovskii [49] form:

$$\rho_{xx}(T) = \rho_0 \exp[(T_0/T)^{1/2}], \quad (1)$$

where  $\rho_0$  and  $T_0$  are fitting parameters. The values for  $T_0$  range from  $T_0 = 50$  K for sample N7 to  $T_0 = 2$  K for N5, typical of amorphous insulating materials [50]. The lowest measurement temperatures accessible for the insulating films are  $\sim T_0$ ; hence we cannot conclusively establish the presence of a Coulomb gap. However, both samples N6 and N7 are

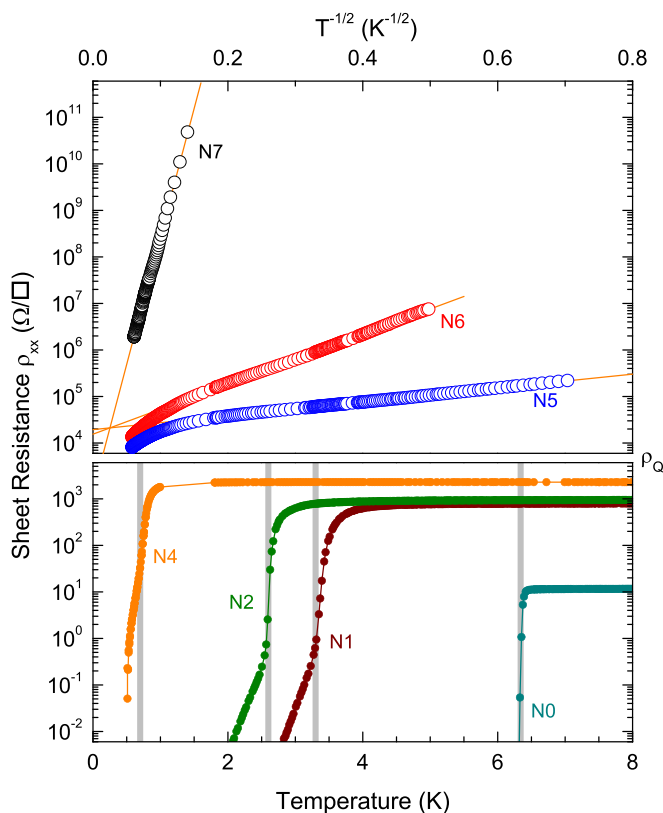


FIG. 4. Sheet resistance  $\rho_{xx}$  of insulating TaN $_x$  films (upper panel) versus  $T^{-1/2}$ ; the linear behavior is consistent with Efros-Shklovskii hopping transport arising from a depletion of the electronic density of states due to Coulomb interactions. Superconducting films (lower panel) show a crossover from 3D to 2D behavior, and finite-size effects appearing as a tail below  $T_c$  (gray bars); lines are guides to the eye.

strongly localized insulators with clear hopping transport, and sample N5 is a marginal insulator; none of the insulating films show activated behavior characteristic of the insulating state adjacent to superconductivity in, e.g., InO $_x$  [29,51].

Less disordered films (N0–N4) with lower nitrogen content  $x$  (or increased thickness) show quantum-corrected metallic behavior below 20 K, with temperature-dependent conductivity contributions  $\Delta\sigma(T) \sim \frac{e^2}{\pi h} \ln(T)$  from weak antilocalization and disorder-enhanced Coulomb interactions in the normal state. Similar  $\ln(T)$  temperature dependence is observed in the normal-state dependence of  $\rho_{xy}(T)$ .

The lower panel of Fig. 4 highlights the superconducting transition at  $T_c$  for the samples shown, which ranges from  $T_{c0} \sim 6.35$  K (sample N0) to 0.5 K (sample N4). With increasing disorder, the  $T_c$  of samples N1–N4 is suppressed; this can be attributed to the effect of enhanced Coulomb interactions [52], as demonstrated in MoGe [53,54]. The increase in disorder arises both from reducing film thickness (samples N0, N1, and N2) and increasing nitrogen composition  $x$  between samples N2, N4, and (insulating) N5. Resistive transitions are broadened due to enhanced superconducting fluctuation conductivity above  $T_c$  [37]. Below  $T_c$ , the superconducting films all show a “foot” arising from a cutoff in the diverging correlation length  $\xi$  due to film inhomogeneity [55] or finite magnetic field [56]; further details of the superconducting properties of these films can be found in Ref. [52].

#### V. FIELD-TUNED SIT

Superconductivity can be suppressed with application of critical fields  $\mu_0 H_{c2} \approx 1$ –5 T, revealing an insulating normal state as  $T \rightarrow 0$ . Figure 5(a) [Fig. 5(b)] shows magnetoresistance isotherms for sample N4 (N3) at temperatures near  $T_c = 0.5$  K (0.7 K); the approximate value for  $H_c$  is indicated with an arrow. For  $H < H_c$  the samples are superconducting;  $\rho_{xx}$  decreases with decreasing temperature. At high magnetic fields  $\rho_{xx}$  shows insulating behavior, diverging as  $T \rightarrow 0$ . While the values for  $H_c$  differ for samples N3 and N4 due to their compositions (N3 is almost pure Ta, while N4 is approximately stoichiometric  $a$ -TaN $_x$ ), the qualitatively similar behavior near the field-tuned transition demonstrates that the film stoichiometry is not a disruptive tuning parameter.

The field-tuned transition between superconducting and insulating temperature dependencies is shown for sample N2 in Fig. 5(c), which plots  $\rho_{xx}$  versus  $T$  curves in zero field and in applied fields of up to 6 T. The low-field curves show superconducting behavior with the value of  $T_c$  gradually suppressed with increasing magnetic field; the 6 T trace shows a negative slope  $d\rho/dT$  to the lowest temperature available,  $\sim 100$  mK, with  $\rho_{xx} \sim \ln(T)$  again as expected for a quantum-corrected diffusive system. This insulating behavior persists unchanged with increasing magnetic fields.

At  $H_c$  there exists a temperature-independent crossing point, whose appearance is a hallmark of the SIT. In the “dirty boson” scenario for the SIT, the behavior near this quantum phase transition is described by the localization of Cooper pairs (or proliferation of vortices) in the presence of disorder at  $H_c$ . Tuning via magnetic field across the putative quantum critical point at  $H_c$  allows us to investigate the critical scaling behavior in its vicinity.

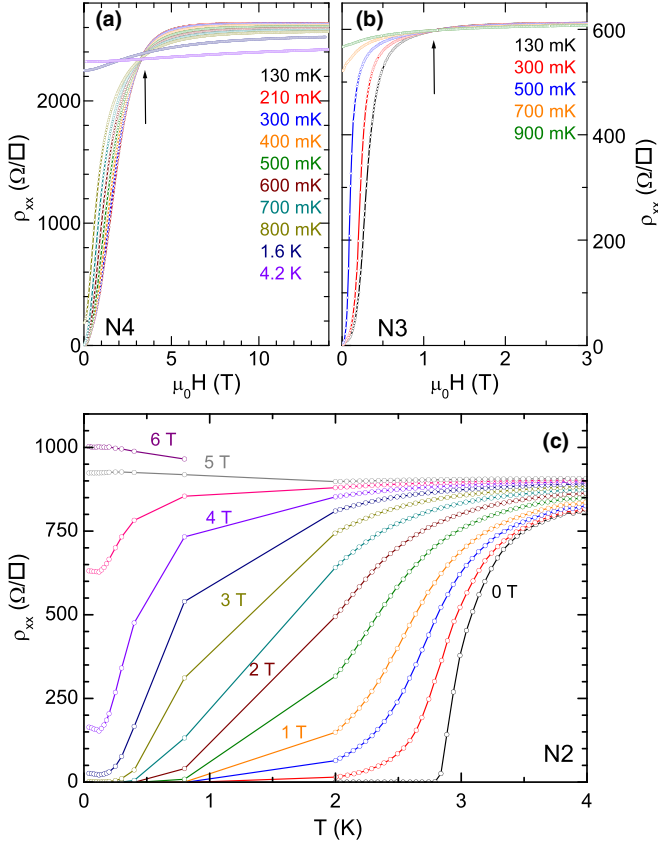


FIG. 5. (a), (b) Magnetic field-tuned SIT in disordered  $a$ - $\text{TaN}_x$  films, evidenced by magnetoresistance isotherms for films N4 and N3. (c) Sheet resistance for sample N2 is plotted as a function of temperature for magnetic fields between 0 and 6 T as indicated, in equal steps. Lines are guides to the eye.

## VI. SCALING NEAR THE SIT

Having identified an apparent SIT in films where disorder has already suppressed  $T_c$  below the bulk value  $T_{c0}$ , we investigate the critical scaling behavior in the vicinity of the critical field  $H_c$  [57,58]. Approaching the field-tuned transition (b-SIT) there is a diverging correlation length  $\xi \sim (H - H_c)^{-\nu}$  with critical exponent  $\nu$ . Nonzero temperatures cut off the vanishing frequency scale  $\Omega \propto \xi^{-z}$ , creating an additional length scale  $L_{\text{th}} = (\hbar/k_B T)^{1/z}$  (here  $z$  is the dynamic critical exponent). Observables such as  $\rho_{xx}$  or  $\rho_{xy}$  must (in 2D) be a universal function  $\tilde{f}$  of the ratio  $\xi/L_{\text{th}}$ , through

$$\rho_{xx}(H, T) = \rho_c \tilde{f}\left(\frac{H - H_c}{T^{1/z\nu}}\right), \quad (2)$$

where  $\rho_c$  is the critical resistance at the transition, predicted in the dirty boson scenario to be  $\rho_c = \rho_Q \equiv \frac{h}{4e^2}$ . Thus isotherms of  $\rho_{xx}$  (or  $\rho_{xy}$ ) should collapse above and below the b-SIT when plotted versus the scaling parameter  $\eta \equiv \frac{H - H_c}{T^{1/z\nu}}$ . The best collapse determines the product  $z\nu$ .

Figure 6 illustrates such finite-size scaling for three  $a$ - $\text{TaN}_x$  films, N2–N4. At left the raw magnetoresistance isotherms (in steps in temperature as indicated) cross at a common critical resistance  $\rho_c$ , with values ranging from 0.6–2.3 k $\Omega$ , all well below  $\rho_Q$ . At right in Fig. 6 are the same data versus the scaling

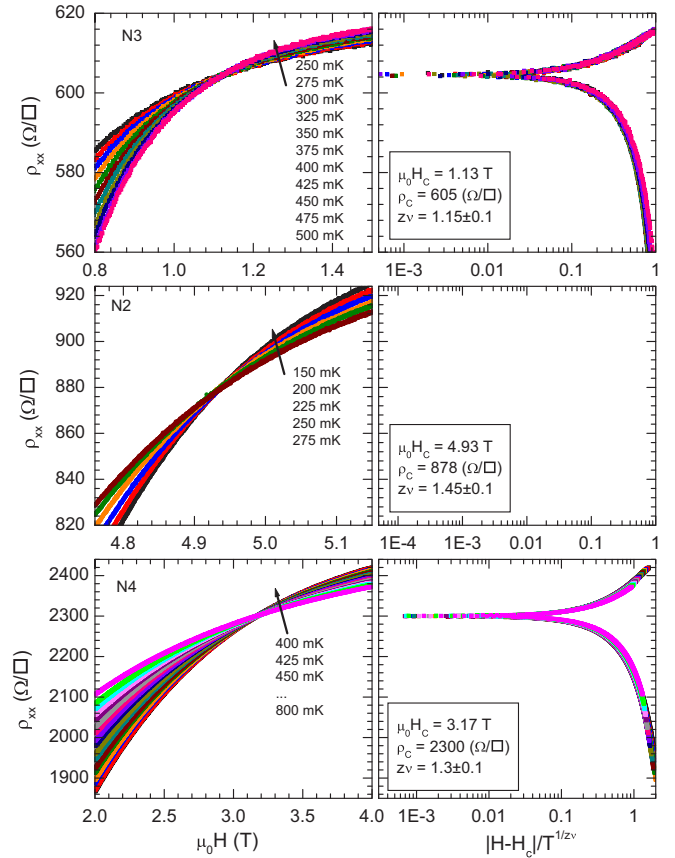


FIG. 6. Left panels: Magnetoresistance isotherms for samples N3, N2, and N4 near the b-SIT. Right panels: Resistance versus the scaling parameter  $\eta$  for the identical data sets plotted at left, showing excellent collapse for a range of temperatures; collected scaling parameters are shown.

parameter  $\eta$ . All three samples exhibit excellent scaling near  $H_c$  over a range of temperatures (for sample N2) well below  $T_c$ , and for samples N3 and N4 approximately up to  $T_c$ , with values of  $z\nu \approx 1.25$ . The scaling is disrupted at the lowest temperatures; such behavior has been seen previously in, e.g., MoGe [3] and InO $_x$  [51]. We also note that values for  $H_c$  are comparable to  $H_{c2}$  estimated for each of these samples (collected in Table II). As discussed further below, these results are consistent with the “weak insulating” behavior seen in previous studies across a range of materials (and a range of disorder strengths) [10]. In none of these studies, however, has

TABLE II. Critical  $a$ - $\text{TaN}_x$  film parameters at the SIT.  $\rho_{xx}^n$  is the resistance in the normal state,  $T_c$  is the transition temperature,  $\rho_c$  and  $H_c$  are the critical resistance and field at the transition,  $H_{c2}(0)$  is an estimate for the mean-field upper critical field, and  $z$  and  $\nu$  are critical exponents.

Sample	$\rho_{xx}^n$ (k $\Omega$ )	$T_c$ (K)	$\rho_c$ (k $\Omega$ )	$\mu_0 H_c$ (T)	$\mu_0 H_{c2}(0)$ (T)	$z\nu$
N2	0.950	2.8	0.880	4.93	5.0	$1.45 \pm 0.1$
N3	0.58	0.5	0.605	1.13	1.2	$1.15 \pm 0.1$
N4	2.4	0.7	2.30	3.17	3.5	$1.30 \pm 0.1$

similar scaling behavior been resolved in the Hall resistance  $\rho_{xy}$ ; we consider such data in the next section.

## VII. HALL EFFECT

Early studies by Paalanen *et al.* [36] found a crossing point in  $\rho_{xy}$  in strongly disordered  $\text{InO}_x$  films beyond  $H_c$ . The investigators hypothesized that this crossing reflected the disappearance of the bosonic insulating behavior. Initial theoretical description of the dirty bosons scenario predicted scaling in  $\rho_{xy}$  in analogy with  $\rho_{xx}$ , with a universal value for  $\rho_{xy}^c$ :

$$\rho_{xy}(H, T) = \rho_{xy}^c \tilde{F}\left(\frac{H - H_c}{T^{1/z\nu}}\right) \quad (3)$$

where again  $\tilde{F}$  is a universal function, and  $\rho_{xy}^c$  was predicted to have a universal value. Subsequent analyses suggested that, due to “hidden” particle-hole symmetry,  $\rho_{xy}^c$  should vanish at the transition [59]. Despite ongoing debate as to the nature of the SIT, there have been no further systematic studies of  $\rho_{xy}$  in its vicinity. This is in part due to the challenge of measuring

$\rho_{xy}$  in materials where high carrier densities  $n$  lead to small signal sizes.

Early scaling theory [57] also predicted that (in the case of a self-dual transition) the value of  $\rho_{xy}^c$  would, together with the critical longitudinal resistance  $\rho_c$ , be given by

$$(\rho_{xy}^c)^2 + \rho_c^2 = \rho_Q^2. \quad (4)$$

Given that  $\rho_{xy}$  is typically much less than  $\rho_Q$  for noninsulating films, this would lead to the strong prediction of  $\rho_c = \rho_Q$  that has been seen in many, but certainly not all, materials. However, in the weakly disordered  $a\text{-TaN}_x$  films considered here, with large  $n$ ,  $R_H \ll 1 \Omega/T$ , and thus  $\rho_{xy} \ll 1 \Omega$ , Eq. (4) would suggest that  $\rho_c \approx \rho_Q$ . As seen in the previous section,  $\rho_c \ll \rho_Q$  for all films at the field-tuned SIT, demonstrating that the nonuniversal  $\rho_c$  in  $a\text{-TaN}_x$  cannot be explained by Eq. (4). Alternatively, a nonuniversal critical Hall resistance may be estimated as  $\rho_{xy}^c = \rho_c \tan(\theta_H)$ , where  $\theta_H$  is the normal-state Hall angle.

Figure 7 shows  $\rho_{xy}$  across the field-tuned SIT in film N2 (lower panel), along with simultaneously measured  $\rho_{xx}$  (upper panel). The scale for  $\rho_{xy}$  has been enlarged to highlight the crossing in  $\rho_{xy}$  traces at  $5.3 \pm 0.1$  T; this is above  $\mu_0 H_c \approx 4.9$  T found in the previous section. (The apparent crossing around 4.3 T does not invert the temperature order of the isotherms, nor does it exhibit good scaling.) The normal-state Hall angle for sample N2 is  $\tan(\theta_H) = 7 \times 10^{-5}$  at 4.9 T, so  $\rho_c \tan(\theta_H) \approx 0.07 \Omega$ , below but comparable to  $\rho_{xy}^c = 0.105 \Omega$ . Following Eq. (3) we plot the scaled  $\rho_{xy}$  in the inset of Fig. 7. As with  $\rho_{xx}$ , the critical Hall resistance  $\rho_{xy}^c$  is not universal; it is well below  $\rho_Q$  and also well below the prediction  $\rho_{xy}^c = 0.99 \times \rho_Q$  of Eq. (4).

## VIII. DISCUSSION AND SUMMARY

Having identified both disorder- and field-tuned SIT in  $a\text{-TaN}_x$ , we can immediately address several of the key open questions surrounding this field. First, the critical disorder for the disorder suppression of superconductivity appears to be coincident with the disorder-driven (Anderson) metal-insulator transition. These  $\text{TaN}_x$  films show a metal-insulator transition as a function concentration  $x$ , with a critical value  $x_c \sim 1.7$  and a critical resistivity comparable to that observed here [47]. This coincidence is seen in  $\text{NbSi}$  [32] and  $\text{NbN}$  [31], and indicates for the SIT observed in these systems a direct link between the appearance of (fermionic) Anderson localization in the normal state and the SIT.

Second, the superconductor–weak-insulator transition (SWIT) observed in  $a\text{-TaN}_x$  appears to be a universal phenomenon. Although the appearance of a true  $T = 0$  quantum phase transition is obscured by the poor scaling and unconventional metallic phase, an increasing number of materials show this phenomenology including  $\text{MoGe}$ ,  $\text{Ta}$ , some  $\text{InO}_x$  films, and others. In particular, critical scaling (with  $z\nu \sim 1.25 \pm 0.25$ ) is comparable to the critical exponent for classical percolation  $z\nu = 4/3$ ,  $H_c \sim H_{c2}(0)$ , and  $\rho_c \ll \rho_Q$  [10]. The presence of metallic ( $n > 10^{22} \text{ cm}^{-3}$ ) carrier densities appears to separate these materials from  $\text{InO}_x$  and related systems that show Bose-insulator behavior. Progress towards a coherent theoretical picture for the dissipative state [23] will need to take this strong sensitivity to  $n$  into account.

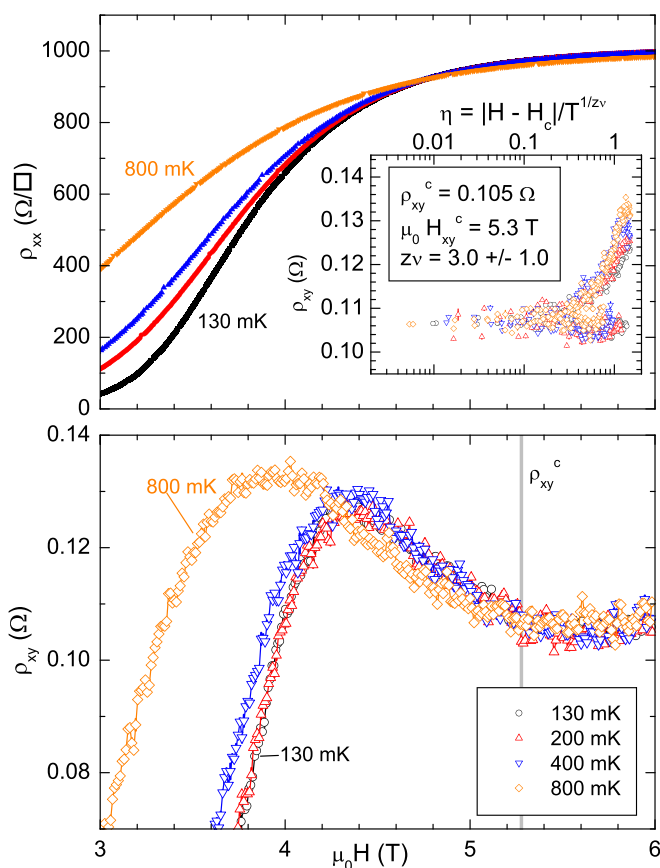


FIG. 7. Sheet resistance  $\rho_{xx}$  (upper panel) and Hall resistance  $\rho_{xy}$  (lower panel) versus magnetic field for  $\text{TaN}_x$  film N2. The magnetoresistance isotherms show a crossing point indicative of a field-tuned SIT; a similar crossing point can be seen in  $\rho_{xy}$  (lower panel). The Hall resistance shows weak scaling in the vicinity of the crossing point  $\rho_{xy}^c$  (gray bar), shown in the inset. Lines are guides to the eye.

Third, we have found evidence for critical scaling in an observable complementary to  $\rho_{xx}$ —the Hall effect. While quantum critical scaling phenomena have been studied extensively using  $\rho_{xx}$  in disordered thin films, similar studies using  $\rho_{xy}$  (or other transport quantities, such as the Nernst effect) are lacking. Here  $\rho_{xy}$  shows a temperature-independent crossing point just above  $H_c$ , whose nature remains unclear. Its value at the transition  $\rho_{xy}^c$  is nonuniversal and well below  $\rho_Q$ , contrasting with the apparent universality of  $\rho_c \sim \rho_Q$  in the strong-disorder limit. As the uncertainty of our results is limited by experimental resolution, future work may both improve the scaling analysis of  $\rho_{xy}$  and track the evolution of  $H_{xy}^c$  as a function of disorder.

Fourth and finally, disorder in these “SWIT” materials cannot be linked to any macroscopic granularity or inhomogeneity. Thorough investigation of the  $a$ -TaN<sub>x</sub> films showed no sign of any length scale for granular behavior in the composition or film structure. In the future, local spectroscopic probes may be necessary to study inhomogeneity length scales in the zero-temperatures phases near the SIT.

In summary, we have identified several features of the SIT in the tunable materials system  $a$ -TaN<sub>x</sub>. Varying

the nitrogen content or reducing film thickness gradually suppresses superconductivity and drives a disorder-tuned SIT. Weakly insulating films with disorder-suppressed  $T_c$  can be tuned via magnetic field through the SIT, and show signatures of the critical behavior arising from an underlying quantum critical point. Films with varying degrees of disorder show scaling consistent with classical percolation, with scaling disrupted at intermediate fields as  $T \rightarrow 0$ . Both  $\rho_{xx}$  and  $\rho_{xy}$  show nonuniversal critical resistances at the SIT, and the Hall effect shows weak scaling at a critical field close to  $H_c$ . Thus,  $a$ -TaN<sub>x</sub> appears to represent a broad class of materials that show rich physics adjacent to the SIT that is distinct from the “classical” picture of disordered bosons.

#### ACKNOWLEDGMENTS

We thank the staff of the Stanford Nanocharacterization Laboratory for exhaustive characterization assistance. Initial work was supported by National Science Foundation Grant No. NSF-DMR-9508419. This work is supported by the Department of Energy, Office of Science, Basic Energy Sciences, Materials Sciences and Engineering Division, under Contract DE-AC02-76SF00515.

- 
- [1] A. M. Goldman and N. Markovic, Superconductor-insulator transitions in the two-dimensional limit, *Phys. Today* **51**(11), 39 (1998).
- [2] V. Dobrosavljevic, N. Trivedi, and J. M. Valles Jr., *Conductor-Insulator Quantum Phase Transitions* (Oxford University Press, Oxford, 2012); S. Sachdev, *Quantum Phase Transitions*, 2nd ed. (Cambridge University Press, Cambridge, 2011).
- [3] N. Mason and A. Kapitulnik, Dissipation Effects on the Superconductor-Insulator Transition in 2D Superconductors, *Phys. Rev. Lett.* **82**, 5341 (1999).
- [4] V. Yu. Butko and P. W. Adams, Quantum metallicity in a two-dimensional insulator, *Nature (London)* **409**, 161 (2001).
- [5] T. I. Baturina, C. Strunk, M. R. Baklanov, and A. Satta, Quantum Metallicity on the High-Field Side of the Superconductor-Insulator Transition, *Phys. Rev. Lett.* **98**, 127003 (2007).
- [6] E. Abrahams, P. W. Anderson, D. C. Licciardello, and T. V. Ramakrishnan, Scaling Theory of Localization: Absence of Quantum Diffusion in Two Dimensions, *Phys. Rev. Lett.* **42**, 673 (1979).
- [7] M. D. Stewart, A. Yin, J. M. Xu, and J. M. Valles, Superconducting pair correlations in an amorphous insulating nanohoneycomb film, *Science* **318**, 1273 (2007).
- [8] H. Q. Nguyen, S. M. Hollen, M. D. Stewart, J. Shainline, A. Yin, J. M. Xu, and J. M. Valles, Observation of Giant Positive Magnetoresistance in a Cooper Pair Insulator, *Phys. Rev. Lett.* **103**, 157001 (2009).
- [9] R. Crane, N. P. Armitage, A. Johansson, G. Sambandamurthy, D. Shahar, and G. Grüner, Survival of superconducting correlations across the two-dimensional superconductor-insulator transition: A finite-frequency study, *Phys. Rev. B* **75**, 184530 (2007).
- [10] M. A. Steiner, N. P. Breznay, and A. Kapitulnik, Approach to a superconductor-to-Bose-insulator transition in disordered films, *Phys. Rev. B* **77**, 212501 (2008).
- [11] M. Ovadia, D. Kalok, B. Sacepe, and D. Shahar, Duality symmetry and its breakdown in the vicinity of the superconductor-insulator transition, *Nat. Phys.* **9**, 415 (2013).
- [12] N. P. Breznay, M. A. Steiner, S. A. Kivelson, and A. Kapitulnik, Self-duality and a Hall-insulator phase near the superconductor-to-insulator transition in indium-oxide films, *Proc. Natl. Acad. Sci. USA* **113**, 280 (2016).
- [13] A. Yazdani and A. Kapitulnik, Superconducting-Insulating Transition in Two-Dimensional  $a$ -MoGe Thin Films, *Phys. Rev. Lett.* **74**, 3037 (1995).
- [14] D. Ephron, A. Yazdani, A. Kapitulnik, and M. R. Beasley, Observation of Quantum Dissipation in the Vortex State of a Highly Disordered Superconducting Thin Film, *Phys. Rev. Lett.* **76**, 1529 (1996).
- [15] Y. Qin, C. L. Vicente, and J. Yoon, Magnetically induced metallic phase in superconducting tantalum films, *Phys. Rev. B* **73**, 100505 (2006).
- [16] W. Liu, L. Pan, J. Wen, M. Kim, G. Sambandamurthy, and N. P. Armitage, Microwave Spectroscopy Evidence of Superconducting Pairing in the Magnetic-Field-Induced Metallic State of InO<sub>x</sub> Films at Zero Temperature, *Phys. Rev. Lett.* **111**, 067003 (2013).
- [17] Y. Saito, Y. Kasahara, J. Ye, Y. Iwasa, and T. Nojima, Metallic ground state in an ion-gated two-dimensional superconductor, *Science* **350**, 409 (2015).
- [18] A. W. Tsen, B. Hunt, Y. D. Kim, Z. J. Yuan, S. Jia, R. J. Cava, J. Hone, P. Kim, C. R. Dean, and A. N. Pasupathy, Nature of the quantum metal in a two-dimensional crystalline superconductor, *Nat. Phys.* **12**, 208 (2016).
- [19] E. Shimshoni, A. Auerbach, and A. Kapitulnik, Transport through Quantum Melts, *Phys. Rev. Lett.* **80**, 3352 (1998).
- [20] A. Kapitulnik, N. Mason, S. A. Kivelson, and S. Chakravarty, Effects of dissipation on quantum phase transitions, *Phys. Rev. B* **63**, 125322 (2001).

- [21] B. Spivak, A. Zyuzin, and M. Hruska, Quantum superconductor-metal transition, *Phys. Rev. B* **64**, 132502 (2001).
- [22] M. Mulligan and S. Raghu, Composite fermions and the field-tuned superconductor-insulator transition, *Phys. Rev. B* **93**, 205116 (2016).
- [23] R. A. Davison, L. V. Delacrétaz, B. Goutéraux, and S. A. Hartnoll, Hydrodynamic theory of quantum fluctuating superconductivity, *Phys. Rev. B* **94**, 054502 (2016).
- [24] N. P. Breznay and A. Kapitulnik, Particle-hole symmetry reveals failed superconductivity in the metallic phase of two-dimensional superconducting films, *Sci. Adv.* **3**, e1700612 (2017).
- [25] Y. Wang, I. Tamir, D. Shahar, and N. P. Armitage, A Bose metal has no cyclotron resonance, [arXiv:1708.01908](https://arxiv.org/abs/1708.01908).
- [26] C. A. Marrache-Kikuchi, H. Aubin, A. Pourret, K. Behnia, J. Lesueur, L. Bergé, and L. Dumoulin, Thickness-tuned superconductor-insulator transitions under magnetic field in  $\alpha$ -NbSi, *Phys. Rev. B* **78**, 144520 (2008).
- [27] T. I. Baturina, D. R. Islamov, J. Bentner, C. Strunk, M. R. Baklanov, and A. Satta, Superconductivity on the localization threshold and magnetic-field-tuned superconductor-insulator transition in TiN films, *JETP Lett.* **79**, 337 (2004).
- [28] M. Mondal, A. Kamlapure, M. Chand, G. Saraswat, S. Kumar, J. Jesudasan, L. Benfatto, V. Tripathi, and P. Raychaudhuri, Phase Fluctuations in a Strongly Disordered  $s$ -Wave NbN Superconductor Close to the Metal-Insulator Transition, *Phys. Rev. Lett.* **106**, 047001 (2011).
- [29] G. Sambandamurthy, L. W. Engel, A. Johansson, and D. Shahar, Superconductivity-Related Insulating Behavior, *Phys. Rev. Lett.* **92**, 107005 (2004).
- [30] T. I. Baturina, A. Yu. Mironov, V. M. Vinokur, M. R. Baklanov, and C. Strunk, Localized Superconductivity in the Quantum-Critical Region of the Disorder-Driven Superconductor-Insulator Transition in TiN Thin Films, *Phys. Rev. Lett.* **99**, 257003 (2007).
- [31] M. Chand, G. Saraswat, A. Kamlapure, M. Mondal, S. Kumar, J. Jesudasan, V. Bagwe, L. Benfatto, V. Tripathi, and P. Raychaudhuri, Phase diagram of the strongly disordered  $s$ -wave superconductor NbN close to the metal-insulator transition, *Phys. Rev. B* **85**, 014508 (2012).
- [32] O. Crauste, F. Couëdo, L. Bergé, C. A. Marrache-Kikuchi, and L. Dumoulin, Destruction of superconductivity in disordered materials: A dimensional crossover, *Phys. Rev. B* **90**, 060203 (2014).
- [33] Y. Seo, Y. Qin, C. L. Vicente, K. S. Choi, and J. Yoon, Origin of Nonlinear Transport across the Magnetically Induced Superconductor-Metal-Insulator Transition in Two Dimensions, *Phys. Rev. Lett.* **97**, 057005 (2006).
- [34] Y. Li, C. L. Vicente, and J. Yoon, Transport phase diagram for superconducting thin films of tantalum with homogeneous disorder, *Phys. Rev. B* **81**, 020505 (2010).
- [35] S. Park, J. Shin, and E. Kim, Scaling analysis of field-tuned superconductor-insulator transition in two-dimensional tantalum thin films, *Sci. Rep.* **7**, 42969 (2017).
- [36] M. A. Paalanen, A. F. Hebard, and R. R. Ruel, Low-Temperature Insulating Phases of Uniformly Disordered Two-Dimensional Superconductors, *Phys. Rev. Lett.* **69**, 1604 (1992).
- [37] N. P. Breznay, K. Michaeli, K. S. Tikhonov, A. M. Finkel'stein, M. Tendulkar, and A. Kapitulnik, Hall conductivity dominated by fluctuations near the superconducting transition in disordered thin films, *Phys. Rev. B* **86**, 014514 (2012).
- [38] N. P. Breznay and A. Kapitulnik, Observation of the ghost critical field for superconducting fluctuations in a disordered TaN thin film, *Phys. Rev. B* **88**, 104510 (2013).
- [39] H. B. Nie, S. Y. Xu, S. J. Wang, L. P. You, Z. Yang, C. K. Ong, J. Li, and T. Y. F. Liew, Structural and electrical properties of tantalum nitride thin films fabricated by using reactive radio-frequency magnetron sputtering, *Appl. Phys. A* **73**, 229 (2001).
- [40] C.-S. Shin, Y.-W. Kim, D. Gall, J. E. Greene, and I. Petrov, Phase composition and microstructure of polycrystalline and epitaxial TaN<sub>x</sub> layers grown on oxidized Si(001) and MgO(001) by reactive magnetron sputter deposition, *Thin Solid Films* **402**, 172 (2002).
- [41] S. Noda, K. Tepsanongsuk, Y. Tsuji, Y. Kajikawa, Y. Ogawa, and H. Komiyama, Preferred orientation and film structure of TaN films deposited by reactive magnetron sputtering, *J. Vac. Sci. Technol. A* **22**, 332 (2004).
- [42] K. Wakasugi, M. Tokunaga, T. Sumita, H. Kubota, M. Nagata, and Y. Honda, Superconductivity of reactivity sputtered TaN film for ULSI process, *Phys. B (Amsterdam, Neth.)* **239**, 29 (1997).
- [43] F. M. Kilbane and P. S. Habig, Superconducting transition temperatures of reactively sputtered films of tantalum nitride and tungsten nitride, *J. Vac. Sci. Technol.* **12**, 107 (1975).
- [44] V. G. Prokhorov, Dependence of the superconducting transition temperature on the thickness of superconducting films with different coherence lengths, *Low Temp. Phys.* **24**, 410 (1998).
- [45] C.-S. Shin, D. Gall, Y.-W. Kim, P. Desjardins, I. Petrov, J. E. Greene, M. Oden, and L. Hultman, Epitaxial NaCl structure  $\delta$ -TaN<sub>x</sub>(001): Electronic transport properties, elastic modulus, and hardness versus N/Ta ratio, *J. Appl. Phys.* **90**, 2879 (2001).
- [46] T. Riekkinen and J. Molarius, Reactively sputtered tantalum pentoxide thin films for integrated capacitors, *Microelectron. Eng.* **70**, 392 (2003).
- [47] L. Yu, C. Stampfl, D. Marshall, T. Eshrich, V. Narayanan, J. M. Rowell, N. Newman, and A. J. Freeman, Mechanism and control of the metal-to-insulator transition in rocksalt tantalum nitride, *Phys. Rev. B* **65**, 245110 (2002).
- [48] D. B. Haviland, Y. Liu, and A. M. Goldman, Onset of Superconductivity in the Two-Dimensional Limit, *Phys. Rev. Lett.* **62**, 2180 (1989).
- [49] A. L. Efros and B. I. Shklovskii, Coulomb gap and low temperature conductivity of disordered systems, *J. Phys. C* **8**, L49 (1975).
- [50] R. Rosenbaum, Crossover from Mott to Efros-Shklovskii variable-range-hopping conductivity in In<sub>x</sub>O<sub>y</sub> films, *Phys. Rev. B* **44**, 3599 (1991).
- [51] M. Steiner and A. Kapitulnik, Superconductivity in the insulating phase above the field-tuned superconductor-insulator transition in disordered indium oxide films, *Phys. C (Amsterdam, Neth.)* **422**, 16 (2005).
- [52] N. P. Breznay, PhD. thesis, Stanford University, 2013.
- [53] A. M. Finkel'shtein, Superconducting transition temperature in amorphous films, *Pis'ma Zh. Eksp. Teor. Fiz.* **45**, 37 (1987) [*JETP Lett.* **45**, 46 (1987)].

- [54] J. M. Graybeal and M. R. Beasley, Localization and interaction effects in ultrathin amorphous superconducting films, *Phys. Rev. B* **29**, 4167 (1984).
- [55] L. Benfatto, C. Castellani, and T. Giamarchi, Broadening of the Berezinskii-Kosterlitz-Thouless superconducting transition by inhomogeneity and finite-size effects, *Phys. Rev. B* **80**, 214506 (2009).
- [56] J. W. P. Hsu and A. Kapitulnik, Superconducting transition, fluctuation, and vortex motion in a two-dimensional single-crystal Nb film, *Phys. Rev. B* **45**, 4819 (1992).
- [57] M. P. A. Fisher, Quantum Phase Transitions in Disordered Two-Dimensional Superconductors, *Phys. Rev. Lett.* **65**, 923 (1990).
- [58] M. P. A. Fisher, G. Grinstein, and S. M. Girvin, Presence of Quantum Diffusion in Two Dimensions: Universal Resistance at the Superconductor-Insulator Transition, *Phys. Rev. Lett.* **64**, 587 (1990).
- [59] M. P. A. Fisher, Hall effect at the magnetic-field-tuned superconductor-insulator transition, *Phys. A (Amsterdam, Neth.)* **177**, 553 (1991).